CLASP regulates mitochondrial distribution in *Schizosaccharomyces pombe*

Stéphane Chiron, Alyona Bobkova, Haowen Zhou, and Michael P. Yaffe

Section of Cell and Developmental Biology, Division of Biological Sciences, University of California, San Diego, La Jolla, CA 92093

Movement of mitochondria in *Schizosaccharomyces pombe* depends on their association with the dynamic, or plus ends, of microtubules, yet the molecular basis for this interaction is poorly understood. We identified *mmd4* in a screen of temperature-sensitive *S. pombe* strains for aberrant mitochondrial morphology and distribution. Cells with the *mmd4* mutation display mitochondrial aggregation near the cell ends at elevated temperatures, a phenotype similar to mitochondrial defects observed in wild-type cells after microtubule depolymerization. However, microtubule morphology and function appear normal in the *mmd4* mutant. The *mmd4* lesion maps to *peg1*$^{+}$, which encodes a microtubule-associated protein with homology to cytoplasmic linker protein–associated proteins (mammalian microtubule plus end–binding proteins). Peg1p localizes to the plus end of microtubules and to mitochondria and is recovered with mitochondria during subcellular fractionation. This mitochondrial-associated fraction of Peg1p displays properties of a peripherally associated protein. Peg1p is the first identified microtubule plus end–binding protein required for mitochondrial distribution and likely functions as a molecular link between mitochondria and microtubules.

Introduction

Mitochondria proliferate by growth and division and cannot be synthesized de novo, so mitochondrial inheritance is required for cell proliferation. Mitochondrial inheritance and mitochondrial dynamics depend on the movement and positioning of mitochondria at specific cellular locations and on modifications of mitochondrial morphology (Yaffe, 1999; Cerveny et al., 2007). Changes in morphology, including the frequent fusion and fission of mitochondria (Shaw and Nunnari, 2002), are associated with cell cycle progression, alterations in metabolism and environment, and segregation of the organelle during division (Yaffe, 1999; Lee et al., 2007). Although many of the molecular details underlying mitochondrial fusion and division have been elucidated (Okamoto and Shaw, 2005), mechanisms mediating mitochondrial movement and positioning remain poorly understood.

Microtubules facilitate mitochondrial movement in most eukaryotic cells. This function has been characterized best in neurons in which mitochondria travel along axon microtubules using kinesin and dynein (Hollenbeck and Saxton, 2005; Pilling et al., 2006). These molecular motors also mediate mitochondrial movement in other eukaryotic cell types (Tanaka et al., 1998; Fuchs and Westermann, 2005). Microtubules also mediate mitochondrial distribution in *Schizosaccharomyces pombe* (Yaffe et al., 1996), but motors do not appear to be involved (Brazer et al., 2000; Yaffe et al., 2003). Instead, mitochondrial movement depends on microtubule dynamics and on the interaction of mitochondria with the microtubule plus ends in *S. pombe* (Yaffe et al., 2003). The molecular basis for this interaction of mitochondria with dynamic microtubules has been unknown.

To identify components that regulate mitochondrial morphology and distribution in *S. pombe*, we isolated temperature-sensitive (ts) mutants that display aberrant mitochondrial morphology after incubation at an elevated temperature. In this study, we present an analysis of one of these mutants, *mmd4*, and identify a specific microtubule-associated protein that facilitates normal mitochondrial distribution.

Correspondence to Stéphane Chiron: schiron@gmail.com

Abbreviations used in this paper: +TIP, plus end–tracking protein; HSP, high speed pellet; SPB, spindle pole body; ts, temperature sensitive.

Results and discussion

mmd4 cells display defects in mitochondrial morphology and distribution

A novel *S. pombe* mutant, *mmd4*, was isolated by microscopic screening of a collection of ts strains. The *mmd4* mutant displayed mitochondria massed in two aggregates toward the cell ends after 4 h of incubation at 37°C (Fig. 1 A). These aggregations appeared as fragmented mitochondria and very small mitochondrial tubules. In contrast, *mmd4* mutant cells incubated at 25°C, and

The Rockefeller University Press $30.00
J. Cell Biol. Vol. 182 No. 1 41–49
www.jcb.org/cgi/doi/10.1083/jcb.200712147

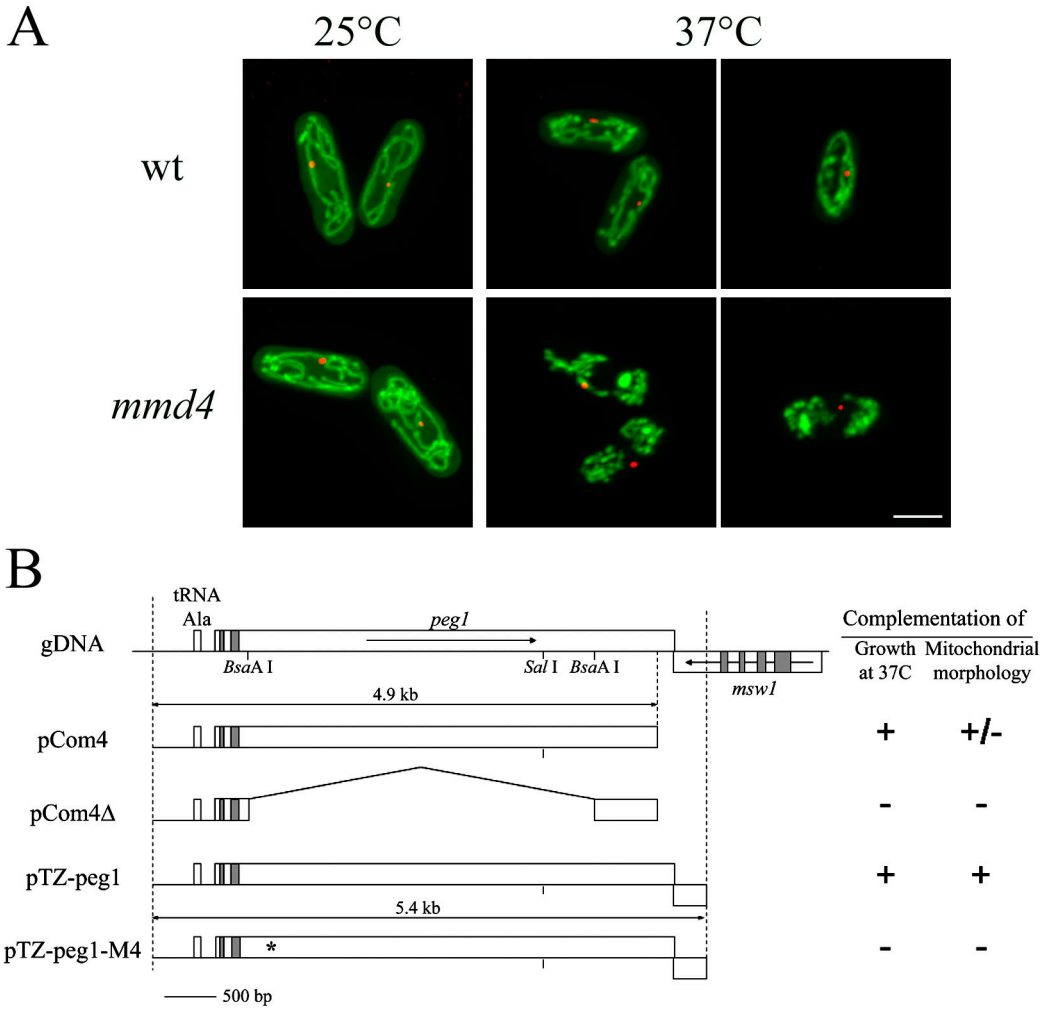

Figure 1. **Mitochondrial morphology in the *mmd4* mutant and identification of *peg1*$^+$.** (A) Wild-type (SCP181-3D) and *mmd4* (SCP181-3A) cells expressing *COX4-GFP* and *sad1-RFP* were observed by confocal microscopy at 25°C and after 4 h at 37°C. Z projections of representative whole cells are shown. Sad1p-RFP was used as a control for interphase cells. (B) The original complementing fragment (pCom4), deletion fragment (pCom4Δ), extended fragment (pTZ-peg1), and mutated fragment (pTZ-peg1-M4) derivatives were introduced in SCP130. Growth and mitochondrial distribution were analyzed after incubation at 37°C. gDNA indicates a map of the genomic vicinity of the *peg1*$^+$ gene. Boxes indicate ORF, and shaded regions represent introns. Arrows show the gene orientations. The asterisk represents the mutation *peg1-M4*. Bar, 5 μm.

wild-type cells grown at either 25 or 37°C contained normal tubular mitochondria distributed throughout the cell (Fig. 1 A).

Genetic analysis involving multiple backcrosses of the *mmd4* mutant to the wild-type parental strain revealed that ts growth and defects in mitochondrial morphology and distribution were caused by a single recessive nuclear mutation. Crosses with *mmd1*, *mmd2*, and *mmd3* mutants confirmed that *mmd4* was a novel mutation defining a gene distinct from those identified in an earlier screen (Weir and Yaffe, 2004).

mmd4 is allelic to *peg1*$^+$, a gene encoding a microtubule-associated protein

To identify the molecular basis for the *mmd4* phenotypes, the *mmd4*$^+$ gene was cloned by complementation of the ts growth defect using a genomic DNA plasmid library. One plasmid, pCom4, was found to complement growth at 37°C and partially restore wild-type mitochondrial morphology. DNA sequencing and comparison of sequences with the *S. pombe* genome database identified the genomic insert as a fragment of chromosome 1, including an alanine-tRNA gene and the 5′ 96% of the *peg1*$^+$ gene (Fig. 1 B). A plasmid derived from pCom4 in which most of *peg1*$^+$ was deleted (pCom4Δ) failed to complement the growth of mutant cells at 37°C, supporting the identity of the complementing activity with *peg1*$^+$.

DNA sequence analysis of the *peg1* gene from both the mutant and wild-type strains revealed a single change in *mmd4* cells, a transition of G to A at nucleotide 370 on the cDNA, resulting in a change of Glu^{124} to Lys. This new *peg1* mutant allele is designated *peg1-M4*.

Further support for the identity of *mmd4* as an allele of *peg1*$^+$ was obtained by examining mutant cells that harbored a second, integrated copy of the gene. The *peg1*$^+$ gene from the genomic insert was completed in the integrative plasmid pTZura4, which was then integrated at the *ura4* locus in *peg1-M4* cells. These cells showed normal growth and mitochondrial morphology at 37°C. When the *peg1-M4* mutation was reintroduced in the pTZ-peg1 plasmid and integrated in the mutant, the resulting transformants displayed all of the mutant phenotypes.

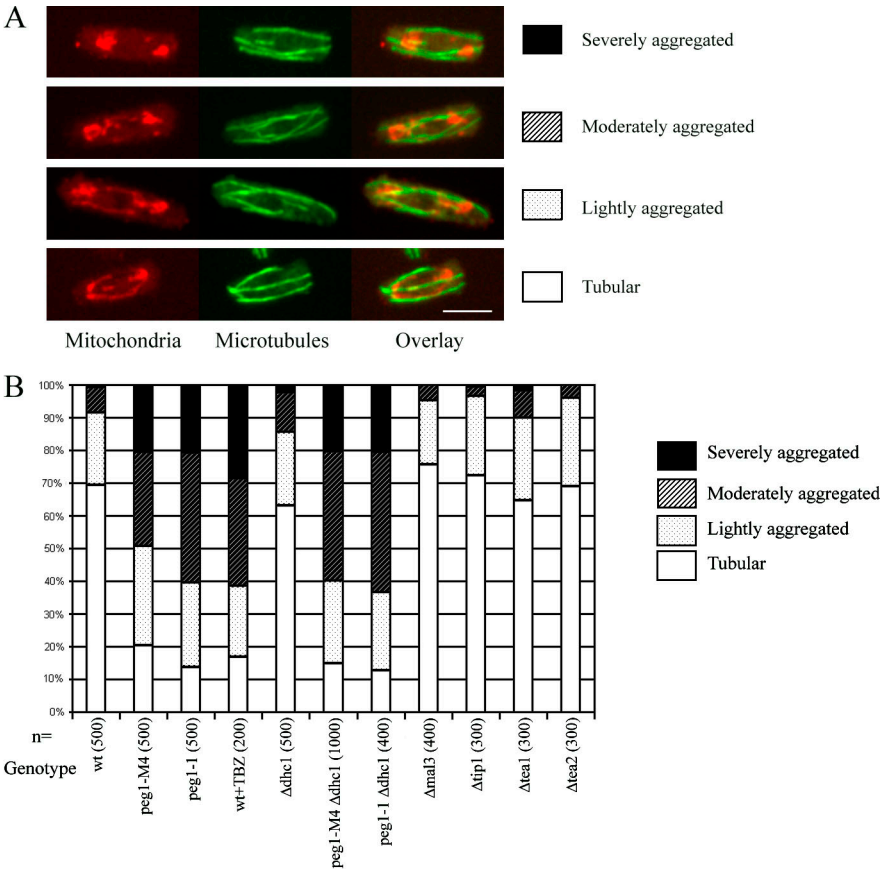

Figure 2. **Morphology of mitochondria and microtubule cytoskeleton.** Indirect immunofluorescence microscopy after 4-h shift at 37°C using the antibodies TAT1 and anti-$F_1\beta$. (A) Representative Z projections of MYP179 cells classified as having severely aggregated, moderately aggregated, lightly aggregated, and predominantly tubular mitochondria. (B) Quantitative analysis of mitochondrial morphology during interphase in the different mutant strains. The strains analyzed include MYP116, MYP179, IH3505, DHC105, SCP177-2C, SCP178-1A, UFY135, ARC1687, and ARC3176. *n*, number of cells analyzed. Bar, 5 µm.

These results confirm that the *peg1-M4* mutation is responsible for the ts growth and mitochondrial morphology defects in the mutant.

The *peg1*$^+$ gene encodes a homologue of the microtubule plus end–tracking proteins (+TIPs) cytoplasmic linker protein–associated proteins (Grallert et al., 2006). The *peg1-1* mutant was previously shown to be defective in the formation of mitotic spindle (Grallert et al., 2006; Bratman and Chang, 2007). Grallert et al. (2006) also reported Peg1p as a destabilization factor for interphase microtubules.

Defects in mitochondrial morphology and distribution caused by *peg1-M4* appear independent of changes in the microtubule cytoskeleton

Microtubules play a central role in mitochondrial morphology and distribution in *S. pombe* (Yaffe et al., 1996), and because Peg1p function has been linked to interphase microtubule dynamics and spindle formation (Grallert et al., 2006; Bratman and Chang, 2007), mitochondrial alterations found in *peg1-M4* cells might be secondary to changes in the microtubule cytoskeleton. To examine this possibility, we analyzed mitochondria and microtubules in *peg1-M4* mutant cells by indirect immunofluorescence after 4 h of incubation at 37°C. Many *peg1-M4* mutant cells displaying microtubule arrays of apparently normal structure show severe defects in mitochondrial distribution and morphology (Fig. 2 A). Further examination of the microtubule morphology revealed an apparent defect in cell cycle progression; 21% of mutant cells incubated at 37°C for 4 h lacked microtubules or contained malformed short spindles, whereas such a phenotype was apparent in only 1% of wild-type cells. However, incubation for 4 h at 37°C did not significantly affect the fraction of cells displaying typical interphase microtubule arrays (76% in the mutant compared with 81% in the wild type).

For quantification of defects in mitochondrial morphology and distribution, cells displaying classic interphase microtubule arrays were assigned to four different classes, including those whose mitochondria were primarily tubular, slightly aggregated, moderately aggregated, and severely aggregated (Fig. 2). In wild-type cells after 4 h at 37°C, 69% of cells ($n = 500$) possess tubular mitochondria, 22% show slight aggregation of mitochondria, 8% have moderate aggregation, and 1% of cells show severe aggregation. In contrast, the *peg1-M4* mutant analysis revealed only 20% of cells ($n = 500$) with tubular mitochondria, 30% with slight aggregation, 29% with moderate aggregation, and 21% with severe aggregation. The same analysis performed on cells harboring the *peg1-1* allele (Grallert et al., 2006) revealed similar defects in mitochondrial morphology and distribution (Fig. 2 B). These results indicate that *peg1* mutations lead to altered mitochondrial morphology and distribution without causing apparent changes in the microtubule cytoskeleton. In contrast to these results, we have analyzed the mitochondrial distribution in wild-type cells after complete microtubule depolymerization by thiabendazole. After 80 min of thiabendazole treatment, cells displayed no microtubules and showed mitochondrial aggregation similar to the *peg1* mutants (Fig. 2 B), indicating that the absence of microtubules can lead to a mitochondrial aggregation similar to the malfunction of Peg1p.

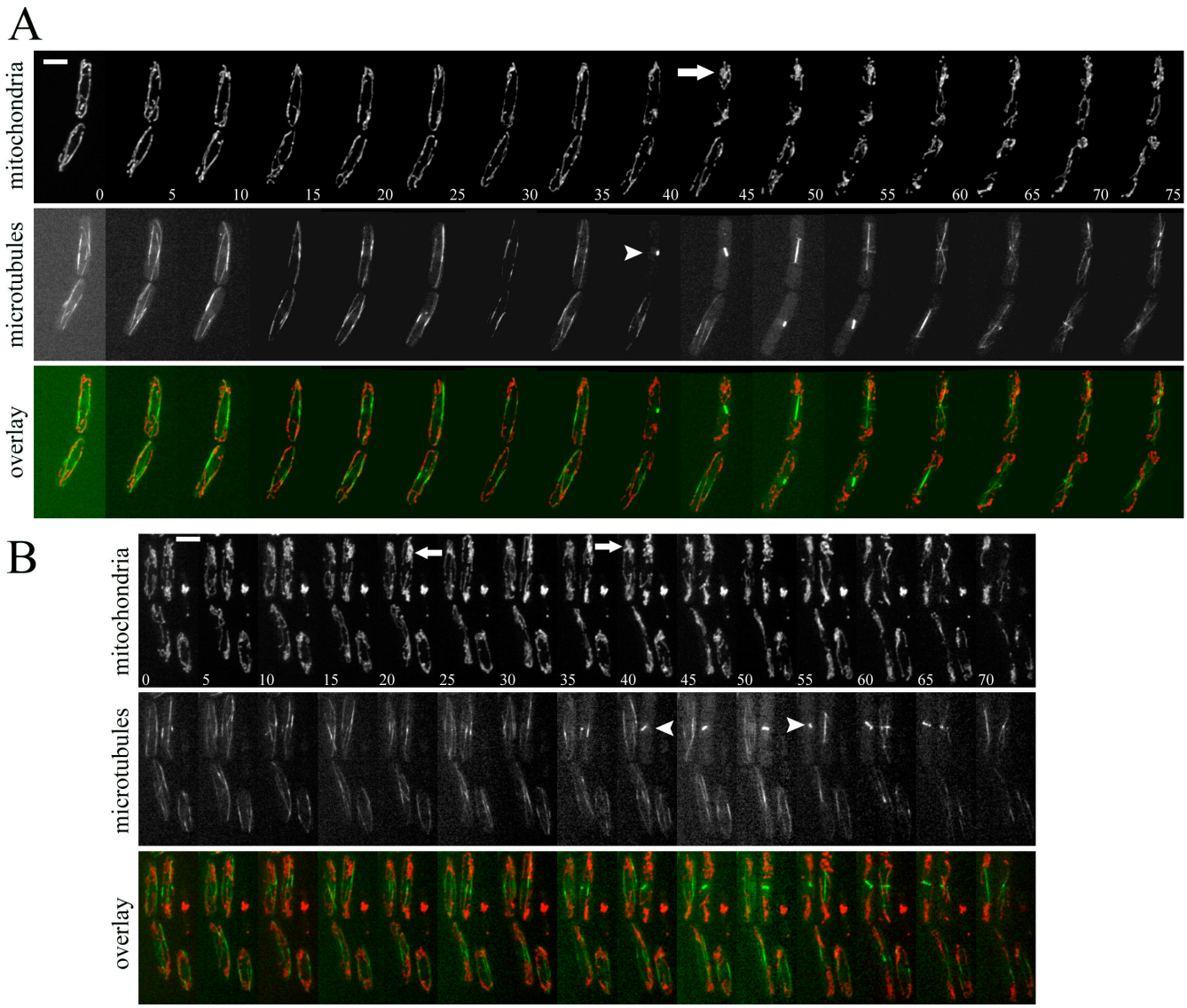

Figure 3. **Development of the *mmd4* mitochondrial phenotype.** Wild-type (A, MYP101) and *peg1-M4* mutant (B, SCP128-2C) were grown at 25°C without thiamine for 48 h and then with thiamine for 16 h and were shifted at 37°C for 2 h. Samples were subjected to time-lapse microscopy at ~37°C. 0.4-µm Z sections were captured at 5-min intervals, and Z projections are shown. Arrows indicate mitochondrial aggregations. Arrowheads identify the initial stage of spindle formation. Bars, 5 µm.

To explore the possibility that minor changes in microtubule dynamics caused by the mutation of *peg1* can contribute to the mitochondrial phenotype, we took advantage of the genetic interaction between the genes *peg1* and *dhc1*. Defects in microtubule dynamics caused by the *peg1-1* mutation were reported to be dependant on dynein function and to disappear when either the light or heavy chain of dynein is deleted (Grallert et al., 2006). Therefore, we examined dynein dependency of the mitochondrial phenotype. Loss of dynein heavy chain (Dhc1p) has been described to have no effect on microtubule morphology or microtubule function during mitosis (Yamamoto et al., 1999). Analysis of the *Δdhc1* mutant revealed no effect on mitochondrial distribution or morphology (Fig. 2 B). However, both double mutants, *peg1-1 Δdhc1* and *peg1-M4 Δdhc1*, show mitochondrial morphology and distribution defects similar to the *peg1* mutants (Fig. 2 B), indicating that the effects of *peg1* on mitochondrial morphology are independent of dynein function. These results further support the conclusion that mitochondrial alterations observed in *peg1* mutant cells are not secondary effects of changes in microtubule dynamics.

Peg1p plays a unique role among +TIPs

Because mitochondrial movement depends on the interaction of mitochondria with the plus ends of microtubules (Yaffe et al., 2003) and Peg1p has been shown to interact with the +TIPs Mal3p and Tip1p (Grallert et al., 2006), we examined whether other +TIPs might contribute to mitochondrial dynamics. Mitochondria were analyzed in cells deleted for *tip1*, *mal3*, *tea1*, or *tea2*. No significant differences in mitochondrial morphology between the mutants and wild-type cells were apparent (Fig. 2 B). The *Δtip1*, *Δmal3*, and *Δtea2* mutants do possess shorter microtubules as previously described (Verde et al., 1995; Beinhauer et al., 1997; Brunner and Nurse, 2000), and consequently, mitochondria in these cells do not extend to the cell ends but are restricted to the areas of growth and shrinkage of the microtubules. However,

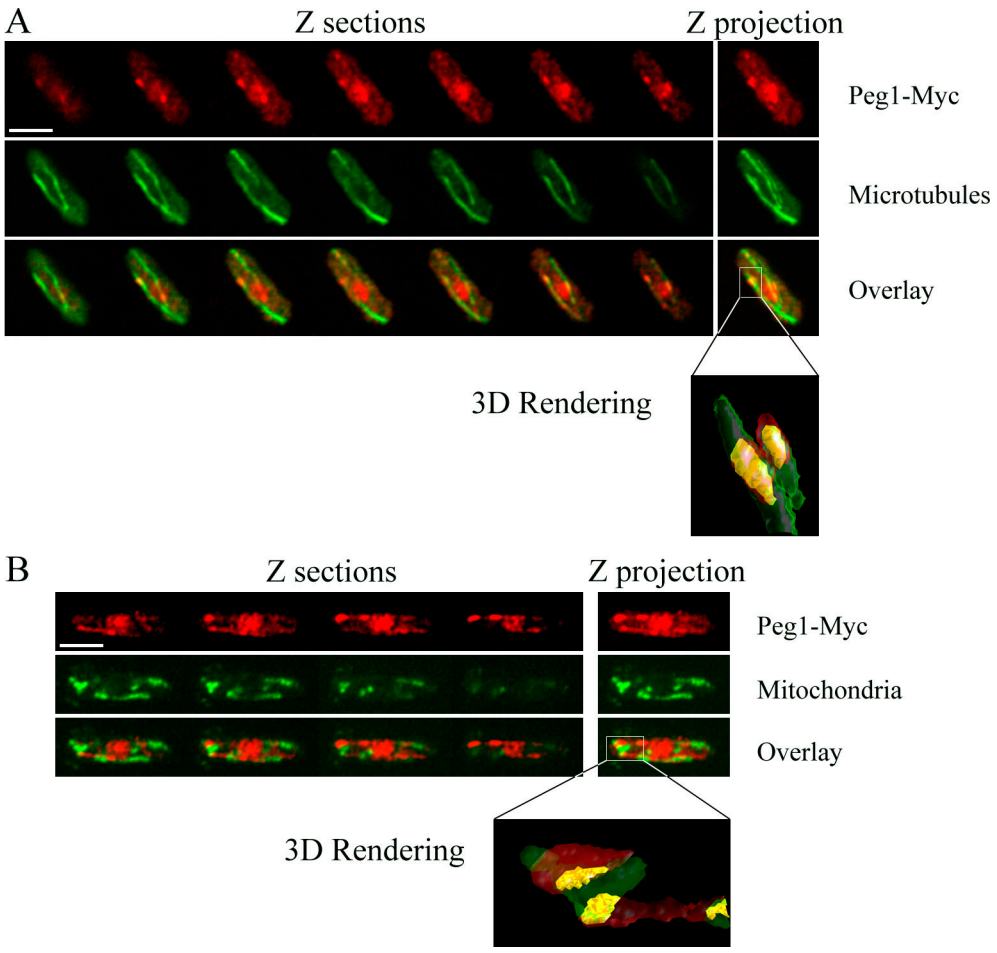

Figure 4. **Microscopic localization of Peg1p.** Indirect immunofluorescence of Peg1p, microtubules, and mitochondria in SCP164 using rabbit anti-myc antibody (A and B) and mAb TAT1 (A) or mAb HSP60 (B). 3DParticles software (Smith et al., 2005) was used to generate the 3D rendering. Bars, 5 µm.

mitochondria in these cells are found as normal tubular structures. Microtubules in *Δtea1* cells are generally longer than wild type (Mata and Nurse, 1997), but defects in mitochondrial morphology and distribution were not observed. These results indicate that Peg1p plays a unique role and appears to be the only microtubule plus end–binding protein to have a direct effect on mitochondrial morphology and distribution in *S. pombe*.

Mitochondrial aggregation in *peg1-M4* cells occurs during interphase

During mitosis in wild-type cells, mitochondria become concentrated toward the cell ends as a consequence of spindle elongation (Yaffe et al., 2003). Because of the similarity of this temporary mitochondrial distribution to the aggregations found in *peg1-M4* mutant cells, we examined whether development of the mutant phenotype required passage through mitosis or was linked to the cell cycle. Live mutant cells with fluorescently tagged mitochondria and microtubules were analyzed by time-lapse confocal microscopy, whereas cells were incubated at the nonpermissive temperature. During the experimental time course with wild-type cells, mitochondria formed a tubular network that extended along the sides of the cell until formation of the spindle (Fig. 3 A, arrowhead). During spindle elongation, mitochondria became aggregated near the cell ends (Fig. 3 A, arrow) until cytoplasmic microtubules reformed, and mitochondria again were distributed throughout the cell. In the *peg1-M4* mutant cells (Fig. 3 B), spindle elongation occurred but was often delayed compared with wild-type cells. In some cells, the spindle failed to elongate for >110 min, whereas other cells formed aberrant spindle structures after a long delay (unpublished data). However, mitochondria became aggregated toward the cell ends (Fig. 3 B, arrows) before spindle formation (Fig. 3 B, arrowheads). These observations indicate that mitochondrial aggregation observed in the *peg1-M4* mutant does not require progression through mitosis and that mitochondrial displacement by the spindle is not required for development of the phenotype.

To confirm the independence of the mitochondrial phenotype from mitotic events, cells were synchronized in interphase by nitrogen starvation, and mitochondria were observed after incubation at 37°C. Mitochondria aggregated in the mutant cells (unpublished data), supporting the conclusion that aberrant mitochondrial distribution is independent of cell cycle progression.

Peg1p localizes to microtubule tips and to mitochondria

Two previous studies addressed the localization of Peg1p, using GFP fusions and CFP or Cherry tubulin constructs (Grallert et al., 2006; Bratman and Chang, 2007). Their conclusions differ

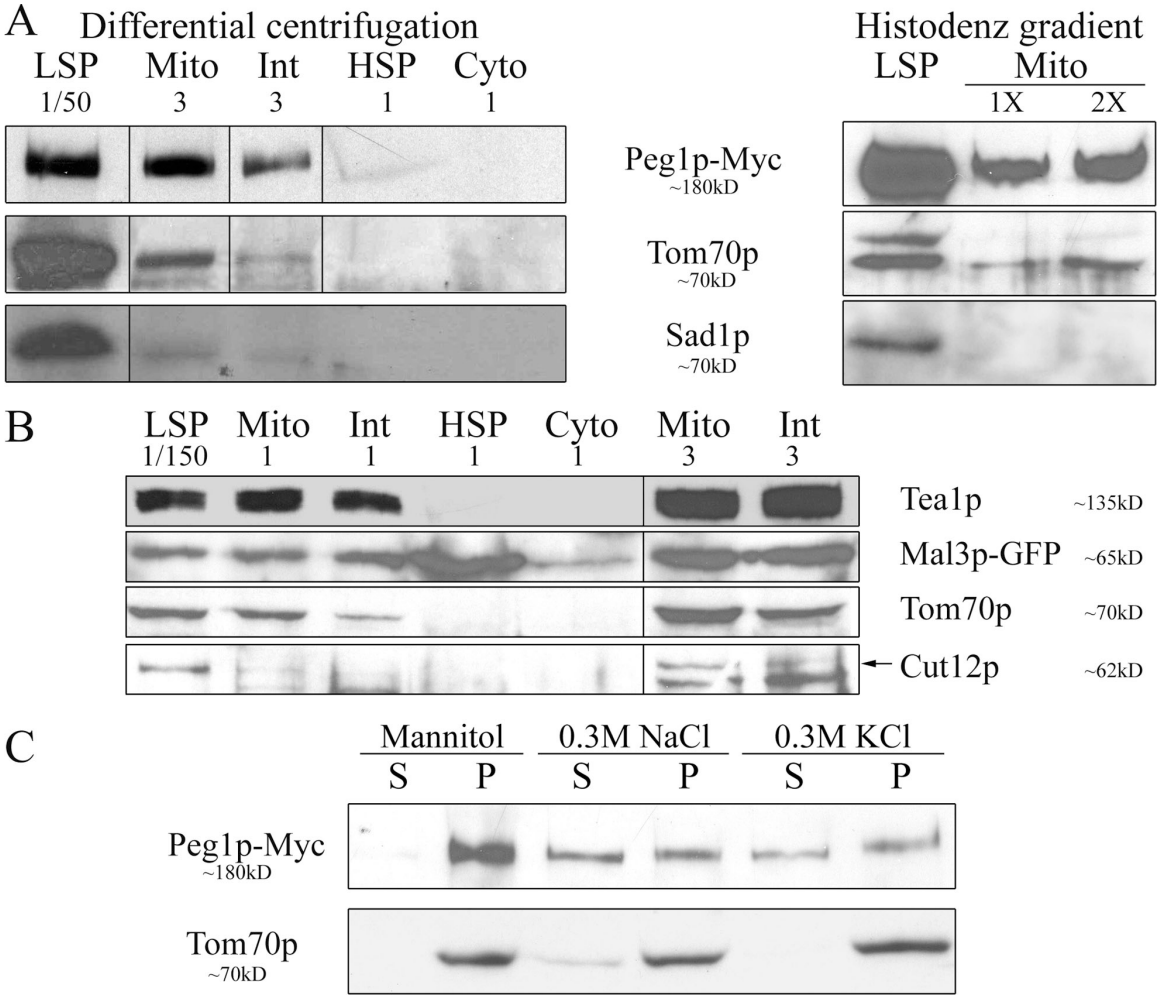

Figure 5. **Peg1p association with mitochondria.** (A) Subcellular fractionation of strain SCP164 by differential centrifugation (left) and mitochondrial purification by banding in a Histodenz gradient (right). Subcellular fractions include low speed pellet (LSP), mitochondria (Mito), intermediate speed pellet (Int), high speed pellet (HSP), and cytoplasm (Cyto). Numbers indicate the relative amount of material (in cell equivalents) loaded on the gel. (B) Fractionation of Tea1p and Mal3-GFP. Strain UFY596 was subjected to subcellular fractionation by differential centrifugation as in A. (C) Mitochondrial membrane association of Peg1p. Mitochondria isolated by differential centrifugation were washed with 0.6 M mannitol solution or the same solution supplemented with 0.3 M NaCl or 0.3 M KCl, and pellet (P) and supernatant (S) fractions were isolated by centrifugation.

concerning the localization of Peg1p on microtubules. In this study, indirect immunofluorescence was used to determine the localization of Peg1p. We constructed a strain expressing a Myc-tagged version of *peg1*$^{+}$ expressed from the endogenous promoter as the only copy of this essential gene. These cells are completely wild type with respect to growth and mitochondrial morphology and distribution (unpublished data). The unavailability of appropriate *S. pombe* antibodies prevented simultaneous localization of Peg1p, mitochondria, and microtubules. Therefore, we assessed the relative localization during interphase of Peg1p with microtubules and with mitochondria individually. As previously reported (Grallert et al., 2006), we found a substantial fraction of Peg1p in the nucleus and also detected the protein at or close to the plus ends of the microtubules (Fig. 4 A). A fraction of cytoplasmic Peg1p was also localized to mitochondria (Fig. 4 B). This mitochondrial-associated Peg1p appeared in discrete patches and punctuate structures rather than being uniformly distributed along mitochondria (Fig. 4 B). These results indicate that Peg1p localizes to both the plus ends of microtubules and to mitochondria. The same localization pattern was observed for Mal3p and Tea1p (unpublished data).

Peg1p is peripherally associated with mitochondria

To further analyze the interaction of Peg1p with mitochondria, the protein was also localized by subcellular fractionation. Cells expressing Myc-tagged Peg1p were homogenized, and the homogenate was fractionated by differential centrifugation. Peg1p was recovered substantially in the mitochondrial fraction together with the mitochondrial marker protein Tom70p (Fig. 5 A, left). Peg1p was also found in the intermediate fraction, which contains some mitochondria, and a trace was detected in the high speed pellet (HSP; Fig. 5 A). A similar mitochondrial localization of Peg1p was detected using an antibody raised against the authentic Peg1p protein (unpublished data).

Peg1p has been shown previously to localize partially in the nucleus and also along the microtubules in the vicinity of the nucleus, with some colocalization with the spindle pole body

Table I. **Yeast strains used in this study**

Strain	Genotype	Source
972h$^-$	*h$^-$*	Yaffe laboratory
FY254	*h$^-$ ade6-M210 ura4-D18 leu1-32 can1-1*	S. Forsburg
FY261	*h$^+$ ade6-M216 ura4-D18 leu1-32 can1-1*	S. Forsburg
JW1084	*h$^-$ ade6-M210 ura4-D18 leu1-32 sad1::mRFP1-Kan^R*	J.Q. Wu
ARC1687	*h$^-$ ura4-D18 Δtea1::ura4+*	P. Nurse[a]
ARC3176	*h$^-$ ade6- ura4-D18 leu1-32 his3-D1 Δtea2::his3+*	P. Nurse[a]
Δtip1	*h$^+$ ura4-D18 Δtip1::Kan^R*	P. Nurse[a]
AY1491-1B	*h$^-$ ade6-210 lys1 ura4 Δdhc1-d4::ura4+*	Yamamoto et al., 1999
DHC105	*h$^+$ his2 ura4 Δdhc1-d2::ura4+*	Yamamoto et al., 1999
OM1602	*h$^-$ ura4-294*	P. Russell[b]
UFY135	*h$^+$ ade6-M210 ura4-D18 leu1-32 his3Δ Δmal3::his3+*	U. Fleig[c]
UFY596	*h$^-$ ade6-M210 ura4-D18 leu1-32 his3D1 mal3-pkGFP:ura4+*	U. Fleig[c]
IH3505	*h$^-$ ura4-D18 leu1-32 peg1-1*	Grallert et al., 2006
641	*h$^-$ ade6-M210 ura4-D18 leu1-32 his3-D1 ars1::nmt-atb1GFP:LEU2*	R. McIntosh[d]
MYP100	*h$^+$ ade6-M216 ura4-D18 leu1-32::nmt1::COX4RFP:leu1+*	Yaffe et al., 2003
MYP115	*h$^-$ ade6-M210 ura4-D18 leu1-32::nmt1::COX4GFP:leu1+*	Weir and Yaffe, 2004
MYP116	*h$^+$ ade6-M216 ura4-D18 leu1-32::nmt1::COX4GFP:leu1+*	Yaffe laboratory
MYP154	*h$^-$ ade6-M210 ura4-D18 leu1-32::nmt1::COX4RFP:leu1+*	Yaffe laboratory
MYP160	*h$^+$ ade6-M216 ura4-D18 leu1-32::nmt1::COX4RFP:leu1+ nmt1::atb1GFP:LEU2*	Yaffe laboratory
MYP179	*h$^+$ ade6-M216 ura4-D18 leu1-32::nmt1::COX4GFP:leu1+ peg1-M4*	EMS mutant of MYP116
SCP119-1C	*h$^-$ ade6-M210 ura4-D18 leu1-32 can1-1 peg1-M4*	Spore from MYP179/FY254
SCP125-4A	*h$^+$ ade6-M216 leu1-32::nmt1::COX4RFP:leu1+*	Spore from MYP100/972h$^-$
SCP126-6A	*h$^+$ ade6-M216 ura4-294 leu1-32::nmt1::COX4RFP:leu1+*	Spore from SCP125-4A/OM1602
SCP127	*h$^+$ ade6-M216 ura4-294 leu1-32::nmt1::COX4RFP:leu1+* *h$^-$ ade6-M210 ura4-D18 leu1-32::nmt1::COX4RFP:leu1+*	Diploid from SCP126-6A/MYP154
SCP128-2C	*h$^+$ ade6-M216 ura4-D18 leu1-32::nmt1::COX4RFP:leu1+ nmt1::atb1GFP:LEU2 peg1-M4*	Spore from SCP119-1C/MYP160
SCP130-1D	*h$^+$ ade6-M216 ura4-294 leu1-32::nmt1::COX4GFP:leu1+ can1-1 peg1-M4*	Spore from MYP179/OM1602
SCP147	*h$^+$ ade6-M216 ura4-294 leu1-32::nmt1::COX4RFP:leu1+ Δpeg1::Kan^R* *h$^-$ ade6-M210 ura4-D18 leu1-32::nmt1::COX4RFP:leu1+*	Transformant of SCP127
SCP164	*h? ade6-M21? ura4-294::pSC144(peg1-13myc):ura4 leu1-32::nmt1::COX4RFP:leu1+ Δpeg1::Kan^R*	Spore of SCP147 + pSC144
SCP177-2C	*h? ade6? Lys1? ura4-D18 leu1-32 Δdhc1-d4::ura4+ peg1-M4*	Spore from MYP179/AY1491-1B
SCP178-1A	*h? ura4-D18 leu1-32 Δdhc1-d2::ura4+ peg1-1*	Spore from IH3505/DHC105
SCP181-3A	*h? ade6? ura4-D18 leu1-32::nmt1::COX4RFP:leu1+ sad1::mRFP1-Kan^R peg1-M4*	Spore from MYP179/JW1084
SCP181-3D	*h? ade6? ura4-D18 leu1-32::nmt1::COX4RFP:leu1+ sad1::mRFP1-Kan^R*	Spore from MYP179/JW1084

[a]The Rockefeller University, New York, NY.
[b]The Scripps Research Institute, La Jolla, CA.
[c]Heinrich-Heine Universität Düsseldorf, Düsseldorf, Germany.
[d]University of Colorado, Boulder, CO.

(SPB; Grallert et al., 2006; Bratman and Chang, 2007). To eliminate the possibility that the mitochondrial Peg1p reflected nucleus and SPB contamination of that fraction, the distribution of Sad1p, a nuclear membrane SPB protein, was also analyzed. Sad1p purified predominantly with the low speed pellet, which contains unbroken cells and nuclei (Fig. 5 A). Only traces of Sad1p were present in the mitochondrial and intermediate fractions. To confirm copurification of Peg1p with the mitochondrial fraction and to eliminate any possible contamination by the nuclear membrane, the mitochondria were further purified by banding on a discontinuous Histodenz gradient. Peg1p copurified with the mitochondrial fraction (Fig. 5 A, right), whereas Sad1p was undetectable in this fraction.

Localization of the two other +TIPs, Tea1p and Mal3p, was also assessed by subcellular fractionation. As with Peg1p, the two +TIPs are substantially recovered in the mitochondrial fraction as well as in the intermediate fraction (Fig. 5 B). Mal3p was also recovered in the HSP. The SPB protein Cut12p is only faintly present in the mitochondrial and intermediate fractions and corresponds to nuclear contamination. These results reveal that the +TIPs Peg1p, Tea1p, and Mal3p copurify with the mitochondrial fraction and suggest an interaction of these proteins with the mitochondria. However, because of the interactions between various +TIPs (Feierbach et al., 2004; Grallert et al., 2006), the recovery of Tea1p and Mal3p in the mitochondrial fraction may occur indirectly via their interaction with Peg1p. The wild-type mitochondrial morphology observed in the absence of Mal3p, Tip1p, or Tea1p indicates that these proteins are not required for mitochondria and microtubule interactions.

To further analyze the association of Peg1p with mitochondria, isolated mitochondria were extracted with sodium chloride and potassium chloride. Washing with either salt led to the recovery of Peg1p in both supernatant and pellet fractions (Fig. 5 C). Under these conditions, the transmembrane protein

Tom70p remains in the pellet fraction. These results demonstrate that a significant fraction of Peg1p displays properties of a peripheral membrane protein.

Our results suggest a model in which Peg1p acts as a linker between mitochondria and microtubules, which is consistent with the recent electron microscopy data (Hoog et al., 2007). Although it could play a supporting role in the loading or assembly of other proteins that actually comprise a molecular bridge, the recovery of Peg1p as a mitochondrial peripheral membrane protein suggests its direct involvement. Such a function as linker between microtubules and membranes has already been documented for the mammalian Peg1p homologues cytoplasmic linker protein–associated proteins in HeLa cells and in motile fibroblasts (Lansbergen et al., 2006). We propose that Peg1p can play a similar role by binding to microtubule plus ends and simultaneously to the mitochondrial outer membrane. The future identification of a mitochondrial membrane protein that serves as a Peg1p receptor and other factors that modulate Peg1p interactions should lead to a more complete understanding of mechanisms that mediate mitochondrial behavior.

Materials and methods

Strains and genetics techniques

The yeast strains used are listed in Table I. Media, growth conditions, and genetic methods for *S. pombe* were described previously (Moreno et al., 1991).

Isolation of *mmd4*

Mutagenesis of *S. pombe* strain MYP116 and isolation of ts mutants displaying mitochondrial defects were performed as previously described (Weir and Yaffe, 2004). Candidate *mmd* mutants were backcrossed three times to the wild-type parental strain, yielding the *mmd4* mutant strain MYP179.

Cloning and analysis of *peg1*$^+$

The *peg1*$^+$ gene was cloned by complementation of the ts phenotype using a pUR19 genomic DNA library (Barbet et al., 1992). The rescuing plasmid, pCom4, was recovered, and the ends of the insert were sequenced. pCom4Δ was created by deleting the 3.4-kb BsaAI fragment. The *peg1*$^+$ gene was completed by PCR in pTZura4 (provided by S. Forsburg, University of Southern California, Los Angeles, CA), yielding to pTZ-peg1. pTZ-peg1M4 was created by in vitro mutagenesis of pTZ-peg1 (QuikChange; Stratagene).

***peg1*$^+$ gene replacement and tagging**

A deletion cassette containing the kanamycin resistance gene flanked by the 5′ (442 bp) and middle (454 bp) regions of *peg1*$^+$ was created in pCRII-TOPO. This cassette, allowing the replacement of *peg1*$^+$ fragment from base 290 to 2,622, was amplified by PCR and transformed into diploid SCP127. The disruption of one copy of *peg1*$^+$ in the resulting strain, SCP147, was confirmed by PCR.

A version of *peg1*$^+$ was engineered to encode Peg1p tagged at its C terminus with 13 copies of the c-myc epitope. A PacI restriction site was created in the STOP codon of *peg1*$^+$ in pTZ-peg1, and the 13Myc of plasmid pFA6a-13Myc-kanMX6 was cloned into PacI. The resulting plasmid, pSC144, was linearized with StuI and transformed into SCP147. Sporulation of the transformant led to haploid segregant SCP164, expressing only a single tagged copy of *peg1* under its own promoter.

Microscopic analysis

Confocal microscopy was performed on a microscope (Axiovert 200M; Carl Zeiss, Inc.) equipped with a Plan-Apochromat 100× NA 1.4 oil objective (Carl Zeiss, Inc.), a spinning disk confocal head (QLC-100; Yokogawa), and an argon/krypton laser (Melles Griot) coupled to an acoustooptical tunable filter (Neos Technologies). Images were captured with a camera (CoolSNAP HQ; Photometrics) and Metavue software (MDS Analytical Technologies). Live cell microscopy was facilitated by the expression of *COX4-GFP* or *COX4-RFP* and/or GFP-tubulin (Yaffe et al., 2003). For time-lapse imaging, cells were recorded on a YES (yeast extract supplemented) agar pad, and the coverslip was sealed with VALAP. For indirect immunofluorescence, cells were fixed by methanol (Hagan and Hyams, 1988). Microtubules were detected using the mouse mAb TAT1 (Woods et al., 1989). Mitochondria were detected with rabbit $F_1\beta$-ATPase antibody (Jensen and Yaffe, 1988) or the mouse mAb HSP60 (Sigma-Aldrich). The c-Myc epitope was detected using the rabbit anti-Myc (Abcam). Secondary antibodies included FITC-conjugated donkey anti–mouse and Texas red–conjugated donkey anti–rabbit (Jackson ImmunoResearch Laboratories).

Subcellular fractionation and biochemical analysis

Subcellular fractions were isolated as previously described (Chiron et al., 2007) with the following modifications. Cells were grown in YES media. The lysis buffer was composed of 0.6 M mannitol and 20 mM Hepes, pH 7.4, supplemented with 1 mM PMSF and protease inhibitor cocktail (Sigma-Aldrich). The pellet from step 13 was saved as the low speed pellet fraction. The supernatant from step 16 was centrifuged at 26,000 *g* for 15 min to yield the intermediate pellet. The supernatant was centrifuged at 164,000 *g* for 1 h to yield an HSP and cytosol fractions. In some experiments, mitochondria were further purified by banding in a Histodenz (Sigma-Aldrich) gradient as described previously (Pagliarini et al., 2005). For mitochondrial elution experiments, isolated mitochondria were treated with 3 vol of lysis buffer supplemented with 0.3 M NaCl or 0.3 M KCl for 10 min at 4°C, and then supernatant and pellet fractions were recovered by centrifugation at 12,000 *g* for 15 min. Western blot analysis was performed using goat anti-Myc (Abcam), rabbit anti-GFP (Affinity BioReagents), Tom70p antibody, Sad1p antibody (provided by M. Shimanuki, Okinawa Institute of Science and Technology, Okinawa, Japan), and Tea1p antibody (Mata and Nurse, 1997).

We thank S. Forsburg, U. Fleig, P. Russell, I. Hagan, K. Gull, M. Shimanuki, and P. Nurse for the gift of strains and antibodies and W. Hu for his assistance.

This work was supported by a United Mitochondrial Disease Foundation grant to S. Chiron and by National Institutes of Health grant GM44614 to M.P. Yaffe.

Submitted: 24 December 2007
Accepted: 6 June 2008

References

Barbet, N., W.J. Muriel, and A.M. Carr. 1992. Versatile shuttle vectors and genomic libraries for use with *Schizosaccharomyces pombe*. *Gene.* 114:59–66.

Beinhauer, J.D., I.M. Hagan, J.H. Hegemann, and U. Fleig. 1997. Mal3, the fission yeast homologue of the human APC-interacting protein EB-1 is required for microtubule integrity and the maintenance of cell form. *J. Cell Biol.* 139:717–728.

Bratman, S.V., and F. Chang. 2007. Stabilization of overlapping microtubules by fission yeast CLASP. *Dev. Cell.* 13:812–827.

Brazer, S.C., H.P. Williams, T.G. Chappell, and W.Z. Cande. 2000. A fission yeast kinesin affects Golgi membrane recycling. *Yeast.* 16:149–166.

Brunner, D., and P. Nurse. 2000. CLIP170-like tip1p spatially organizes microtubular dynamics in fission yeast. *Cell.* 102:695–704.

Cerveny, K.L., Y. Tamura, Z. Zhang, R.E. Jensen, and H. Sesaki. 2007. Regulation of mitochondrial fusion and division. *Trends Cell Biol.* 17:563–569.

Chiron, S., M. Gaisne, E. Guillou, P. Belenguer, D. Clark-Walker, and N. Bonnefoy. 2007. Studying mitochondria in an attractive model: *Schizosaccharomyces pombe*. *Methods Mol. Biol.* 372:91–105.

Feierbach, B., F. Verde, and F. Chang. 2004. Regulation of a formin complex by the microtubule plus end protein tea1p. *J. Cell Biol.* 165:697–707.

Fuchs, F., and B. Westermann. 2005. Role of Unc104/KIF1-related motor proteins in mitochondrial transport in *Neurospora crassa*. *Mol. Biol. Cell.* 16:153–161.

Grallert, A., C. Beuter, R.A. Craven, S. Bagley, D. Wilks, U. Fleig, and I.M. Hagan. 2006. *S. pombe* CLASP needs dynein, not EB1 or CLIP170, to induce microtubule instability and slows polymerization rates at cell tips in a dynein-dependent manner. *Genes Dev.* 20:2421–2436.

Hagan, I.M., and J.S. Hyams. 1988. Use of cell division cycle mutants to investigate the control of microtubule distribution in the fission yeast *Schizosaccharomyces pombe*. *J. Cell Sci.* 89:343–357.

Hollenbeck, P.J., and W.M. Saxton. 2005. The axonal transport of mitochondria. *J. Cell Sci.* 118:5411–5419.

Hoog, J.L., C. Schwartz, A.T. Noon, E.T. O'Toole, D.N. Mastronarde, J.R. McIntosh, and C. Antony. 2007. Organization of interphase microtubules in fission yeast analyzed by electron tomography. *Dev. Cell.* 12:349–361.

Jensen, R.E., and M.P. Yaffe. 1988. Import of proteins into yeast mitochondria: the nuclear MAS2 gene encodes a component of the processing protease that is homologous to the MAS1-encoded subunit. *EMBO J.* 7:3863–3871.

Lansbergen, G., I. Grigoriev, Y. Mimori-Kiyosue, T. Ohtsuka, S. Higa, I. Kitajima, J. Demmers, N. Galjart, A.B. Houtsmuller, F. Grosveld, and A. Akhmanova. 2006. CLASPs attach microtubule plus ends to the cell cortex through a complex with LL5beta. *Dev. Cell.* 11:21–32.

Lee, S., S. Kim, X. Sun, J.H. Lee, and H. Cho. 2007. Cell cycle-dependent mitochondrial biogenesis and dynamics in mammalian cells. *Biochem. Biophys. Res. Commun.* 357:111–117.

Mata, J., and P. Nurse. 1997. tea1 and the microtubular cytoskeleton are important for generating global spatial order within the fission yeast cell. *Cell.* 89:939–949.

Moreno, S., A. Klar, and P. Nurse. 1991. Molecular genetic analysis of fission yeast *Schizosaccharomyces pombe*. *Methods Enzymol.* 194:795–823.

Okamoto, K., and J.M. Shaw. 2005. Mitochondrial morphology and dynamics in yeast and multicellular eukaryotes. *Annu. Rev. Genet.* 39:503–536.

Pagliarini, D.J., S.E. Wiley, M.E. Kimple, J.R. Dixon, P. Kelly, C.A. Worby, P.J. Casey, and J.E. Dixon. 2005. Involvement of a mitochondrial phosphatase in the regulation of ATP production and insulin secretion in pancreatic beta cells. *Mol. Cell.* 19:197–207.

Pilling, A.D., D. Horiuchi, C.M. Lively, and W.M. Saxton. 2006. Kinesin-1 and Dynein are the primary motors for fast transport of mitochondria in *Drosophila* motor axons. *Mol. Biol. Cell.* 17:2057–2068.

Shaw, J.M., and J. Nunnari. 2002. Mitochondrial dynamics and division in budding yeast. *Trends Cell Biol.* 12:178–184.

Smith, W.B., S.R. Starck, R.W. Roberts, and E.M. Schuman. 2005. Dopaminergic stimulation of local protein synthesis enhances surface expression of GluR1 and synaptic transmission in hippocampal neurons. *Neuron.* 45:765–779.

Tanaka, Y., Y. Kanai, Y. Okada, S. Nonaka, S. Takeda, A. Harada, and N. Hirokawa. 1998. Targeted disruption of mouse conventional kinesin heavy chain, kif5B, results in abnormal perinuclear clustering of mitochondria. *Cell.* 93:1147–1158.

Verde, F., J. Mata, and P. Nurse. 1995. Fission yeast cell morphogenesis: identification of new genes and analysis of their role during the cell cycle. *J. Cell Biol.* 131:1529–1538.

Weir, B.A., and M.P. Yaffe. 2004. Mmd1p, a novel, conserved protein essential for normal mitochondrial morphology and distribution in the fission yeast *Schizosaccharomyces pombe*. *Mol. Biol. Cell.* 15:1656–1665.

Woods, A., T. Sherwin, T.H. McRae, A.J. Baines, and K. Gull. 1989. Definition of individual components within the cytoskeleton of *Trypanosoma brucei* by a library of monoclonal antibodies. *J. Cell Sci.* 93:491–500.

Yaffe, M.P. 1999. The machinery of mitochondrial inheritance and behavior. *Science.* 283:1493–1497.

Yaffe, M.P., D. Harata, F. Verde, M. Eddison, T. Toda, and P. Nurse. 1996. Microtubules mediate mitochondrial distribution in fission yeast. *Proc. Natl. Acad. Sci. USA.* 93:11664–11668.

Yaffe, M.P., N. Stuurman, and R.D. Vale. 2003. Mitochondrial positioning in fission yeast is driven by association with dynamic microtubules and mitotic spindle poles. *Proc. Natl. Acad. Sci. USA.* 100:11424–11428.

Yamamoto, A., R.R. West, J.R. McIntosh, and Y. Hiraoka. 1999. A cytoplasmic dynein heavy chain is required for oscillatory nuclear movement of meiotic prophase and efficient meiotic recombination in fission yeast. *J. Cell Biol.* 145:1233–1249. doi:10.1083/jcb.145.6.1233